Electrochemical Lithium Insertion in Zn_3P_2 Zinc Phosphide†

Marie-Pierre Bichat,‡ Jean-Louis Pascal,‡ Frédéric Gillot,§ and Frédéric Favier*,‡

Laboratoire des Agrégats Moléculaires et Matériaux Inorganiques, UMR 5072 CNRS, Université Montpellier II, cc015, 34095 Montpellier Cedex 05, France, and Laboratoire de Réactivité et de Chimie des Solides, UMR-CNRS 6007, Université de Picardie Jules Verne, 33 Rue Saint Leu, 80039 Amiens Cedex, France

Received June 22, 2005. Revised Manuscript Received August 30, 2005

Zn_3P_2 zinc phosphide was synthesized as powders by three different preparation routes: ball-milling, ball-milling followed by annealing, and ceramics at high temperature. Depending on the synthetic route, various powder morphologies (size and crystallinities) were obtained. The electrochemical reactivity toward lithium of these various Zn_3P_2 powders is shown to be unique despite some quantitative performance differences. The insertion mechanism is shown to involve two distinct but parallel reversible pathways for a large number of inserted lithiums (up to nine): one implies exclusively phosphide phases: Zn_3P_2, LiZnP, Li_4ZnP_2, and Li_3P. The second one involves only Li−Zn alloys: Zn, $LiZn_4$, and LiZn. Among these various phases two of them are described for the first time: Li_4ZnP_2 and $LiZn_4$. Both crystal structures have been solved and refined by Rietveld analysis of X-ray diffraction patterns on powders to $R_B = 3.46$ ($R_F = 2.73$, $R_p = 5.71$, $R_{wp} = 7.33$) for Li_4ZnP_2 and to $R_B = 6.70$ ($R_F = 5.23$, $R_p = 6.94$, $R_{wp} = 9.19$) for $LiZn_4$ powders, respectively.

Introduction

The design of new anodes for lithium-ion batteries is a very active research and development field, especially on inorganic compounds as efficient alternatives to carboneous materials.[1] The motivations essentially lie in overcoming performance limitations and patent issues. Systems recently proposed as non-carboneous materials for negative electrode use include CoP_3, InSb, SnO_2, and so forth. These compounds exhibit greater capacities than graphite but usually suffer from a limited capacity retention.[2−4] Among these materials, phosphides represent one of these potentially attractive alternatives. We have shown that transition metal phosphides, such as Li_xMP_4 ternary phases (M = Ti, V, etc.), can actually reversibly insert lithium ions at a potential of about 1 V to lead to quite large capacities up to 900 (m Ah)/g on several cycles.[5,6] However, when incorporated in the usual lithium ion batteries, negative electrodes are not lithiated. The cathode is the lithiated electrode and anode lithiation arises during the charge of the battery. Moreover, lithium presence leads to preparation, safety, and implementing material problems. We have thus been exploring the electrochemical properties of several unlithiated binary metal phosphides such as Cu_3P, CuP_2, CrP, and TiP_2. Among these compounds some just insert a small amount of lithium or the insertion reaction is clearly irreversible. In contrast, Cu_3P has shown more attractive characteristics.[7] Lithium insertion into Cu_3P leads to copper metal extrusion in a reversible process. Electrochemical processes involving such generation of metal nano-inclusions through lithium insertion have also been encountered in InSb, for example.[8,9] As a consequence of this particular insertion mechanism, electrochemical performances of Cu_3P, especially initial capacity and capacity retention, are shown to strongly correlate the powder morphologies.[10] On the other hand, the Zn−P system is a very rich system with several binary phases showing redox properties as well as open structural frameworks favorable to lithium insertion. As a matter of fact, several ternary Li−Zn−P and binary Li−Zn phases are thermodynamically stable.[11] However, for the whole system, information, especially electrochemical and crystallographic data, remains scarce.

The reactivity of lithium with several zinc-based materials, oxides, and intermetallics have recently been studied.[12−15]

† During the manuscript preparation this work was presented by M. P. Bichat at the LiBD-3 conference held in Arcachon, France, 22−27 May 2005 (extended abstract T26, pp 148−149).

* To whom correspondence should be addressed. E-mail: fredf@univ-montp2.fr.

‡ Université Montpellier II.

§ Université de Picardie Jules Verne.

(1) Nazri, G. A.; Pistola, G. In *Lithium batteries: science and technology*; Kluwer Academic Publishers: Dordrecht, The Netherlands, 2003.
(2) Vaughey, J. T.; Kepler, K. D.; Benedek, R.; Thackeray, M. M. *Electrochem. Commun.* **1999**, *1*, 517.
(3) Idota, Y.; Kubota, T.; Matsufuji, A.; Myasaka, T. *Science* **1997**, *276*, 1395.
(4) Retoux, R.; Brousse, T.; Schleich, D. M. *J. Electrochem. Soc.* **1999**, *146*, 2472.
(5) Bichat, M. P.; Gillot, F.; Monconduit, L.; Favier, F.; Morcrette, M.; Lemoigno, F.; Doublet, M. L. *Chem. Mater.* **2004**, *16*, 1002.
(6) Gillot, F.; Bichat, M. P.; Favier, F.; Morcrette, M.; Doublet, M. L.; Monconduit, L. *Electrochim. Acta* **2004**, *49*, 14.
(7) Bichat, M. P.; Politova, T.; Pascal, J. L.; Favier, F.; Monconduit, L. *J. Electrochem. Soc.* **2004**, *151*, A2074.
(8) Vaughey, J. T.; O'Hara, J.; Thackeray, M. M. *Electrochem. Solid State Lett.* **2000**, *3*, 13.
(9) Johnson, C. S.; Vaughey, J. T.; Thackeray, M. M.; Sarakonsri, T.; Hackney, S. A.; Fransson, L.; Edström, K.; Thomas, J. O. *Electrochem. Commun.* **2000**, *2*, 595.
(10) Bichat, M. P.; Politova, T.; Pfeiffer, H.; Tancret, F.; Monconduit, L.; Pascal, J. L.; Brousse, T.; Favier, F. *J. Power Sources* **2004**, *136*, 80.
(11) Gasior, W.; Moser, Z. *J. Chim. Phys. Phys.-Chim. Biol.* **1993**, *90*, 387.
(12) Li, H.; Huang, X.; Chen, L. *Solid State Ionics* **1999**, *123*, 189.

10.1021/cm0513379 CCC: $30.25
Published on Web 11/19/2005

Zinc pnictides, Zn_4Sb_3[16] and Zn_3N_2,[17] have also been evaluated as negative electrode materials. Zinc antimonide, Zn_4Sb_3, reacts with lithium to reversibly form LiZnSb, Li_3Sb, and LiZn. The lithiation reaction with Zn_3N_2 leads to a mixture of LiZn and βLi_3N through the formation of $LiZn_2$ and Li_2Zn_3 alloys. Delithiation is rather complex with the successive involvement of Li_2Zn_3, $LiZn_2$, Li_2Zn_5, an unknown phase, βLi_3N, LiZn, $LiZn_4$, and Zn metal. For both antimonide and nitride, electrode performances, especially cyclability, are however limited. During this manuscript preparation, Satya Kishore and Varadaraju presented a short study on the electrochemical reactivity of Zn_3P_2 toward lithium.[18] Insertion is said to proceed by Zn and phosphorus extractions and formation of amorphous Li_3P. In a second step, extracted Zn metal reacts with lithium to give LiZn at the end of discharge. In charge, LiZn and Li_3P first decomposed under Li extraction and, through a solid-state process, generated elemental Zn and P and then give Zn_3P_2 to achieve the reversibility of the reaction. However, technical limitations from the experimental methodology they used, e.g., ex situ X-ray diffraction, strongly restrained the description of the insertion−extraction mechanism especially on the formation of intermediate phases if any.

A brief overview recently allowed us to identify Zn_3P_2 as the most promising negative electrode material for Li-ion batteries in the Li−Zn−P system.[19] In this paper, we will then describe the lithium reactivity toward Zn_3P_2. Various synthetic routes have been investigated for the preparation of Zn_3P_2 powders: ball-milling without and with annealing and ceramics. The lithium insertion/extraction mechanism and electrode performances are discussed through galvanostatic and potentiodynamic measurements and in situ X-ray diffraction data. The mechanism is shown to strongly differ from those of Zn_4Sb_3 and Zn_3N_2.

1. Experimental Description

1.1. Preparation of Li−Zn−P Powders: Zn_3P_2, LiZnP, Li_4ZnP_2, $LiZn_4$, and LiZn. Reagents: red phosphorus (99% Aldrich) and zinc powder metal (99.9% Alfa Aesar) were used as received. Li_3P was prepared by ball-milling from lithium metal (99.9% Aldrich) and red phosphorus.

Three different synthetic routes were used for the preparation of Zn_3P_2 powders.

With use of a general method described by Juza and coworkers,[20] Zn_3P_2 was prepared at high temperature (herafter HT) from stoichiometric amounts of zinc metal and red phosphorus powders in a sealed silica tube. After a ramp of 1 °C/min, the mixture was kept for 5 days at 850 °C before being quenched in air.

Table 1. Details of Rietveld Refinements for Li_4ZnP_2 (Left) and $LiZn_4$ (Right)[a]

composition	$Li_4Zn\ P_2$	$LiZn_4$
Mr	155.112	268.541
symmetry	cubic	hexagonal
space group	*Fm*3*m* (No. 225)	$P6_3/mmc$ (No. 194)
lattice params (Å, deg)	$a = 5.9035(1)$	$a = 2.7702(8)$
		$c = 4.3785(9)$
Z	2	2
lattice volume (Å^3)	205.74 6(3)	29.09(2)
d(calc) (g/cm^3)	2.508	6.075
X-ray wavelength (Å)	1.5405 6	1.54056
2θ range (deg)	21.0104−113.9848	33.0017−118.3564
step incr (2θ)	0.0334	0.0334
no. of rflns	14	21
no. of atoms	4	2
R_B	3.46	6.70
R_F	2.73	5.23
R_p	5.71	6.94
R_{wp}	7.33	9.19

	x	y	z	B_{iso}	site occ		x	y	z	B_{iso}	site occ
Zn	1/4	1/4	1/4	3.3(1)	0.25	Zn	1/3	2/3	1/4	0.8(2)	0.8
Li	1/4	1/4	1/4	7.4(2)	0.75	Li	1/3	2/3	1/4	1.9(4)	0.2
Li	1/2	1/2	1/2	7.6(2)	0.5						
P	0	0	0	2.3(1)	1						

[a] Atomic coordinates, isotropic displacement parameters, and site occupancies are given in the bottom part of the table.

Ball-milling (BM) has recently been used as a powerful synthetic method for the preparation of electrode materials in lithium-ion batteries.[21] BM syntheses were performed using a Spex 8000 mixer mill that generates mechanical strain. To prepare Li−Zn−P powders, stoichiometric amounts of precursor (Zn metal and red P powders and either lithium metal or Li_3P powder) were placed into a stainless steel container together with steel balls for a weight ratio of steel balls to powder in the range from 8/1 to 10/1. The grinding time for such a precursor mixture was set for 6−12 h for complete reactions. In a typical experiment, 500 mg of products was obtained. The powders were annealed in sealed silica tubes for nonlithiated phases or in stainless steel tubes for lithiated phases at temperature ranging from 150 to 900 °C (temperature ramp of 1 °C/min) for 1−2 weeks before being quenched in air for nonlithiated phases and promptly quenched in liquid air for lithiated phases. Annealed powders are referenced below as BMA.

Hygroscopic and O_2 sensitive reagents and products were stored and handled in a glovebox filled with dry argon (water and oxygen contents <5 ppm).

1.2. X-ray Diffraction on Powder. The grinding vials were opened in a glovebox and the powder purities and crystallinities of prepared Li−Zn−P powders were checked by X-ray diffraction (XRD). Sampling of finely ground and sieved powders was done in Lindeman capillaries (diameter = 0.3 mm) and X-ray diffraction patterns were recorded on a Philips Xpert diffractometer operating with a Cu Kα_1 radiation in the Debye−Scherrer geometry. For Li_4ZnP_2 and $LiZn_4$ powders, specific measurement conditions are reported in Table 1.

1.3. Electrochemical Measurements. Electrochemical tests were performed in Swagelok-type cells assembled in an argon-filled drybox. These cells consist of a composite electrode containing 10−12 mg of active material mixed with 15 wt % of carbon black, a lithium metal disk as counter and reference electrode, and a Whattman GF/D borosilicate glass microfiber separator saturated with a 1 M $LiPF_6$ in ethylene carbonate/dimethylcarbonate (1/1) electrolyte solution (Merck) placed in between. The electrochemical insertion was monitored using a MacPile or a VMP automatic

(13) Belliard, F.; Connor, P. A.; Irvine, J. T. S. *Solid State Ionics* **2000**, *135*, 163.
(14) Alcantara, R.; Tillard-Charbonnel, M.; Spina, L.; Belin, C.; Tirado, J. L. *Electrochim. Acta* **2002**, *47*, 115.
(15) Cao, G. S.; Zhao, X. B.; Li, T.; Lu, C. P. *J. Power Sources* **2001**, *94*, 102.
(16) Zhao, X. B.; Cao, G. S. *Electrochim. Acta* **2001**, *46*, 891.
(17) Pereira, N.; Klein, L. C.; Amatucci, G. G. *J. Electrochem. Soc.* **2002**, *149*, A262.
(18) Satya Kishore, M. V. V. M.; Varadaraju, U. V. *J. Power Sources* **2005**, *144*, 204.
(19) Bichat, M. P.; Monconduit, L.; Pascal, J. L.; Favier, F. *Ionics* **2005**, *11*, 66.
(20) Schlenger, H.; Jacobs, H.; Juza, R. *Z. Anorg. Allg. Chem.* **1971**, *385*, 177.
(21) Gillot, F.; Bichat, M. P.; Favier, F.; Morcrette, M.; Tarascon, J. M.; Monconduit, L. *Ionics* **2003**, *9*, 71.

Table 2. Electrochemical Performances upon Cycling of Zn_3P_2/Li Electrochemical Cells[a]

	specific capacity (mA h/g) after *n* cycles									
	C/13					C/190				
	0.5	1	3	5	10	0.5	1	3	5	10
HT	667	443	440	423	391	995	666	508	309	127
BM	710	556	506	325	98	980	624	373	96	
BMA	617	450	501	502	402	685	420	163	67	

[a] Specific capacitances are given at high (C/13) and low (C/190) scan rates for Zn_3P_2 prepared at high temperature (HT), by ball-milling as prepared (BM) or after annealing (BMA).

cycling/data recording system (Biologic SA, Claix, France) operating in galvanostatic mode in the range 2−0.02 V. With use of the same setup and equipment, potentiodynamic cycling with galvanostatic acceleration measurements have been done at a scan rate of 10 mV/h with a lower current limit corresponding to 1 Li/10 h. Specific capacities obtained for discharge and charge at indicated scan rates are summarized in Table 2.

1.4. In Situ XRD. In situ XRD patterns on powder were collected with a Phillips DA8 diffractometer monochromated Co Kα_1 at various states of charge and discharge of the Zn_3P_2/Li system using a special electrochemical cell. The electrode material was sampled underneath a beryllium window used as current collector. The complete device was then placed in the diffractometer and connected to a MacPile apparatus. Such an experiment was performed in galvanostatic intermittent mode, using current-on periods of 45 min at a scan rate of 1 Li/3 h. Patterns are recorded during current-off periods of 1 h. For sake of clarity and consistency with presented X-ray diffraction patterns of prepared phases, in situ angular data were converted to Cu Kα_1 wavelength.

2. Results

Zn_3P_2 presents two allotropic forms, α and β. α form is tetragonal $P4_2/nmc$ (No. 137), $a = 8.11$ Å, $c = 11.47$ Å[22,23] while β form structure is cubic $P4_232$ (No. 208), $a = 5.68$ Å.[24] Zn atoms are in tetrahedral P-coordinated sites while P atoms are in octahedral Zn-coordinated sites to form, in both structures, alternation of Zn and P layers.[25] We have tried several synthetic routes to prepare these various Zn_3P_2 forms but only the α form has been obtained up to now (Figure 1). As a matter of fact, β form synthesis is said to proceed under pressure (5−40 kbar)[26] and we have been unable to get this phase either by BM or HT routes. The crystallinity of α-Zn_3P_2 powders, hereafter Zn_3P_2, prepared by BM, BMA, and HT was checked by XRD and, despite differences in peak shapes, powder purities were confirmed for the various preparation routes.

Large quantities of lithium were found to react with Zn_3P_2. As shown in Figure 2, galvanostatic curves for the various Zn_3P_2 prepared powders present the same profile over the successive cycles, demonstrating the same mechanism to occur in the whole series and along the cycles. The same observation was made at both applied scan rates, C/13 and C/190, but as usually observed the corresponding capacities however depend on the imposed scan rate. At C/13, the first

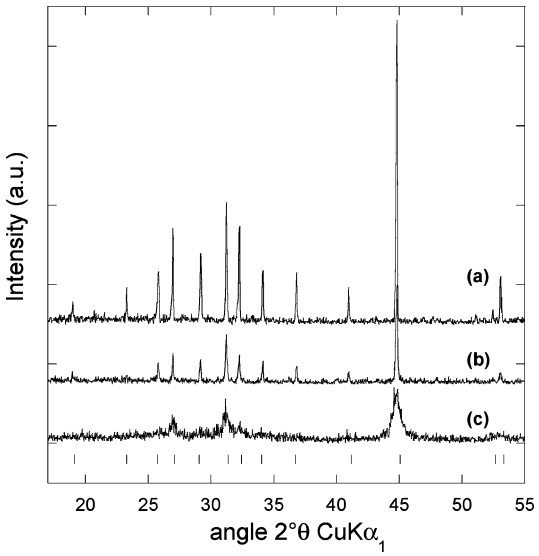

Figure 1. X-ray diffraction of α-Zn_3P_2 powders prepared by various synthetic routes: (a) high temperature (HT); (b) ball-milling followed by annealing (BMA); (c) as prepared by ball-milling (BM). Bars represent Bragg positions for Zn_3P_2 diffraction peaks (JCPDS-22-1021)

specific capacities ranged from 600 to 700 (mA h)/g respectively 2800 to 3200 (mA h)/cm^3, depending on the powder preparation route. A rather large irreversible capacity of 150−200 (mA h)/g (680−910 (mA h)/cm^3), about 20−30% of the initial capacity, is however also observed (Table 2). At C/190 capacities are greater but a lower reversibility was achieved for a capacity loss of up to 30−40% of the initial capacity.

2.1. Li Reaction Followed by in Situ XRD. First discharge in situ XRD pattern series for Zn_3P_2 BMA are depicted in Figure 3a for the reaction of the first 1.5 Li. For the first 0.5 Li, patterns show only diffraction peaks from pure Zn_3P_2 ($P4_2/nmc$ (No. 137), $a = 8.11$ Å, $c = 11.47$ Å).[27] As is usually observed for a solid-solution lithium insertion, a progressive amorphization under lithiation is characterized by an increase in the full width at half-maximum (fwhm) of the Zn_3P_2 peaks. However, the reaction of this 0.5 Li does not induce any peak shifts to lower angles (nor cell volume expansion) as could have been expected for the insertion within the tetragonal Zn_3P_2 structure. Next patterns (from $x = 0.5$ to $x = 1.5$ inserted Li per Zn_3P_2) show the progressive conversion under lithiation of the starting Zn_3P_2 into LiZnP ($F\bar{4}3m$ (No. 216), $a = 5.755$ Å).[28] The formation of Zn metal ($P6_3/mmc$ (No. 194), $a = 2.6591$ Å, $c = 4.9353$ Å)[29] undergoes this conversion as demonstrated by the intensity increase of characteristic diffraction peaks, especially the (1,0,1) peak at 43.47° (2θ). After the reaction of 1.5 Li, the remaining peaks are those of LiZnP and Zn. At this stage Zn_3P_2 conversion is complete and corresponds to the first half of the observed galvanostatic plateau (central inset Figure 3). As shown in Figure 3b, further lithiation, from $x = 1.5$ to $x = 2.25$, leads to the formation of an unknown phase while Zn peak intensities further increase. This lithiation step corresponds to the second part of the galvanostatic plateau and is associated with a two-phase

(22) Von Stackelberg, M.; Paulus, R. *Z. Phys. Chem.* **1935**, *B28*, 427.
(23) Zanin, Y. E.; Aleïnikova, K. B.; Antipin, M. Yu.; Afanas'ev, M. M. *Crystallogr.-Rep.* **2004**, *49*, 579.
(24) Passerini, L. *Gazz. Chim. Ital.* **1928**, *58*, 655.
(25) Andrzejewski, J.; Misiewicz, J. *Phys. Status Solidi B* **2001**, *227*, 515.
(26) Osugi, J.; Tanaka, Y. *Nippon Kagaku Kaishi* **1969**, *90*, 538.
(27) JCPDS 22-1021.
(28) JCPDS 42-1130.
(29) JCPDS 01-1238.

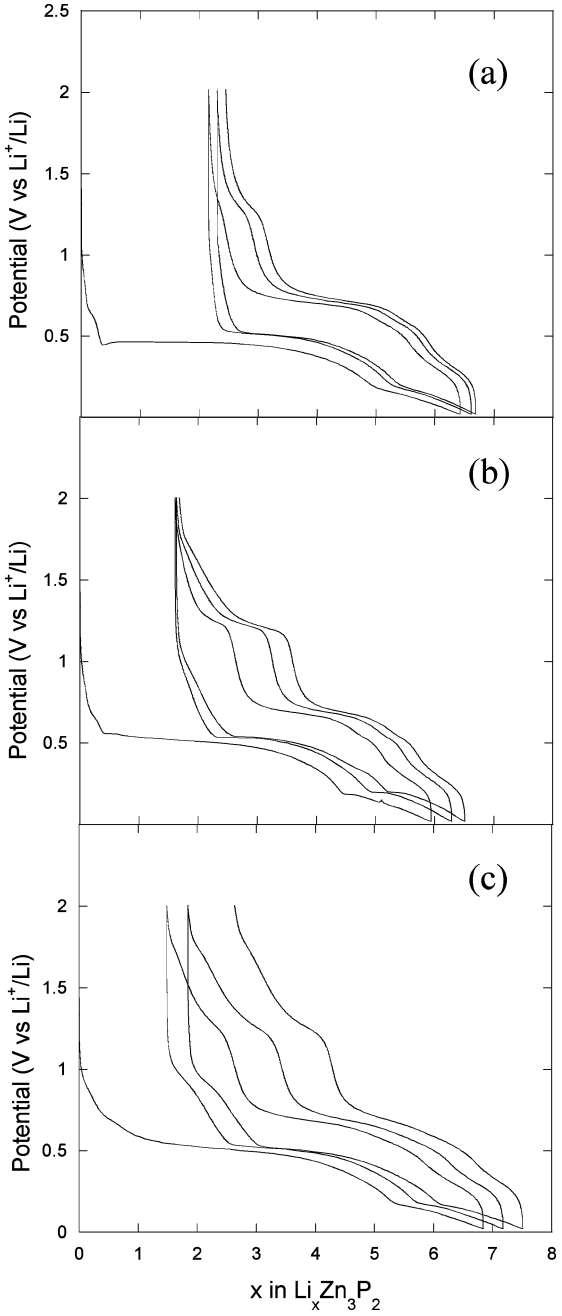

Figure 2. Galvanostatic curves of Zn_3P_2 powders prepared by various synthetic routes: (a) high temperature (HT); (b) ball-milling followed by annealing (BMA); (c) as prepared by ball-milling (BM).

process corresponding to the progressive conversion of LiZnP into Zn metal and a co-generated unknown phase. Since only two products, Zn and this unknown phase, are generated during this conversion, the latter may be a Li-reach ternary phosphide phase with a Li/Zn ratio greater than 1 and Zn/P ratio below 1. Except for Li_9ZnP_4 which we have recently prepared,[19] there is not any known ternary Li−Zn−P phases which could fit these two requirements. Moreover, Li_9ZnP_4 diffraction pattern shows diffraction peaks at 25.85° and 42.87° 2θ in the 20−50 angular range which could fit the unknown phase pattern. This observation is however based on the presence of only two peaks, among which only one is discrete and does not merge any peaks from other included phases. Moreover, Li/Zn = 9 is a ratio pretty higher than expected at such lithiation stage and the diffraction peak measured at 26.15° (2θ) for the unknown phase is slightly higher than the 25.85° we reported for Li_9ZnP_4. On the other hand, among the few A−Zn−P phases reported in the literature (with A = alkalines or alkalines earths), Na_4ZnP_2 shows a A/Zn ratio more consistent with the considered lithiation stage. Unfortunately, Na_4ZnP_2 is an $R\bar{3}m$ (No. 166) rhombohedral phase (a = 5.664 Å, c = 26.101 Å)[30] and its calculated diffraction pattern does not fit the observed diffraction pattern from in situ data, avoiding any helpful isostructural relationship. Moreover, Li_4ZnP_2 is not referenced in any available databases. Despite these discouraging observations, we succeeded in the preparation of Li_4ZnP_2. Li_4ZnP_2 was synthesized by BM from a stoichiometric mixture of Li_3P, Zn, and red phosphorus (from analysis Li/Zn = 4.14 and Zn/P = 0.54). Noteworthy is the fact that it was impossible to obtain Li_4ZnP_2 as a pure phase at high temperature but annealing of the BM powder at 550 °C for 15 days drastically increased the quality of the corresponding diffraction pattern. In Figure 4, a rapid comparison with the in situ data revealed the unknown phase to be Li_4ZnP_2 (as an example, the peak at 26.15° (2θ) in in situ data was measured at 26.13° (2θ) in the Li_4ZnP_2 pattern). The crystal and molecular structure of Li_4ZnP_2 were solved by Rietveld analysis of high-quality X-ray diffraction data on powder and are presented in a next section.

Figure 3c depicting the effects of the insertion of 2.5−3.5 lithium shows the appearance of another unknown phase while Zn quickly disappears and peaks from Li_4ZnP_2 progressively vanish. The new unknown phase presents the same series of diffraction peaks (same intensity ratios) than Zn metal. The observed large shift to higher angles is however characteristic of an isostructural cell with a smaller volume. This kind of topotactic transformation is consistent with alloying processes. The Li−Zn phase diagram has been already described[11] but, unfortunately, among the various reported alloys, LiZn, $LiZn_2$, Li_2Zn_5, Li_2Zn_3, and $LiZn_4$, only LiZn structure has been fully described.[31] The X-ray diffraction pattern for LiZn[32] was found not matching that of the unknown phase and we have then tried to prepare other Li−Zn alloys by BM for structural investigations. On the basis of the absence of diffraction peaks characteristic for both Li and Zn metals, only LiZn and $LiZn_4$ phases were successfully synthesized as pure powders (from analysis Li/Zn = 0.28 for $LiZn_4$). Unlike that of LiZn, $LiZn_4$ diffraction pattern was actually found to match that of the unknown phase. After annealing for 7 days at 150°C of the BM prepared powder, $LiZn_4$ structure was refined by Rietveld analysis of the corresponding X-ray diffraction data (see below). $LiZn_4$ comes from the direct lithiation of Zn nanoparticles generated as phosphide phases are progressively reduced during the charge process. For 2.5 inserted lithium and more, the electrochemical mechanism is then split into two distinct but parallel pathways. One implies exclusively Li−Zn alloys; the other concerns the reduction of Li_4ZnP_2. The former reaction consumes Zn metal simul-

(30) Eisenman, B.; Somer, M. *Z. Naturforsch., B: Chem. Sci.* **1989**, *44*, 1228.
(31) Zintl, E.; Brauer, G. *Z. Phys. Chem.* **1933**, *20B*, 245.
(32) JCPDS 03-0954.

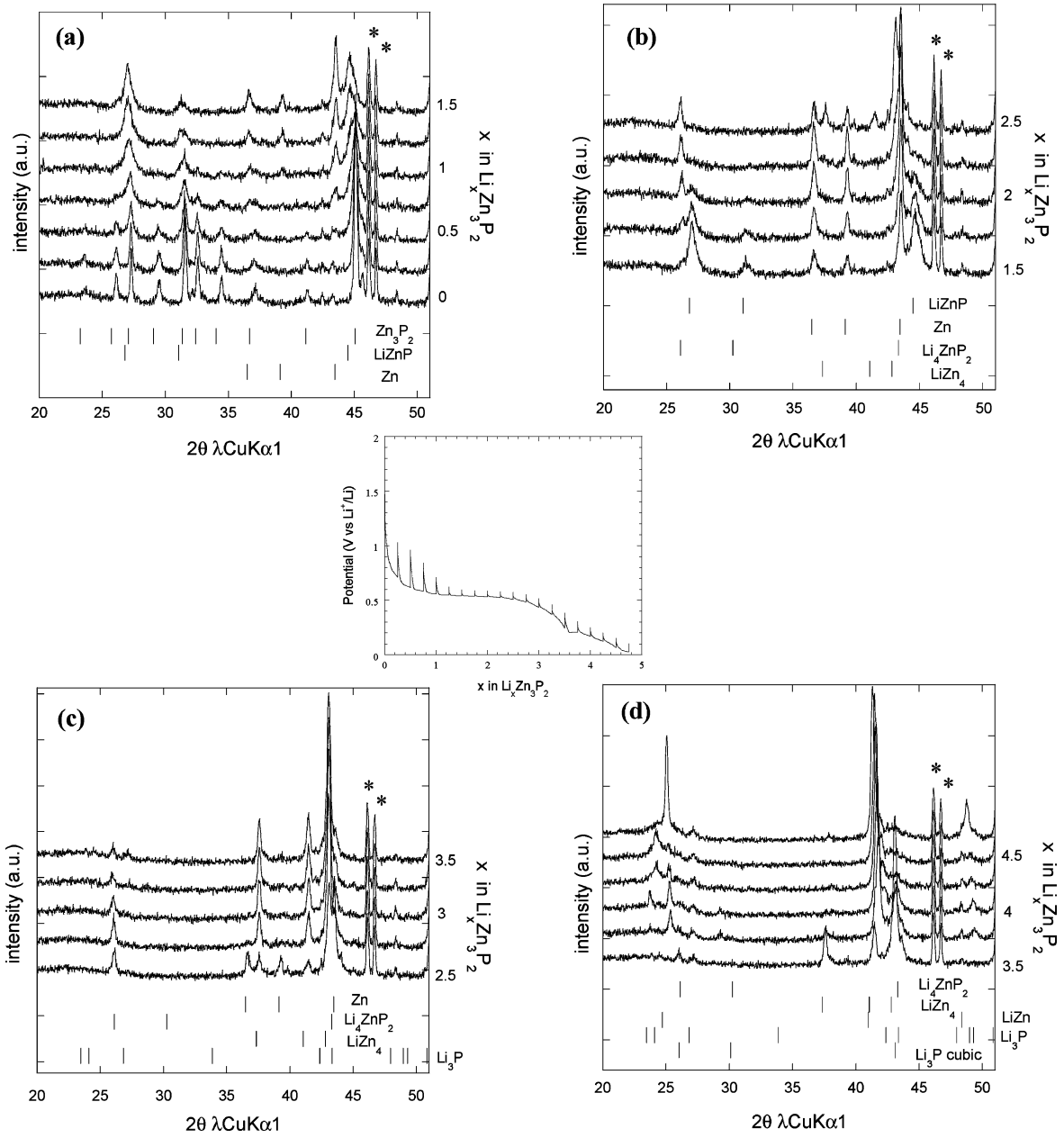

Figure 3. In situ X-ray diffraction patterns collected at various first discharge states of lithiation for Zn_3P_2. Right axis gives corresponding Li composition for $0 < x < 1.5$ in (a), $1.5 < x < 2.5$ in (b), $2.5 < x < 3.5$ in (c), and $3.5 < x < 4.75$ in (d). Bragg peak positions extracted from JCPDS database are given underneath experimental data for involved phases. For Li_4ZnP_2 and $LiZn_4$, Bragg peak positions were extracted from experimental X-ray diffraction data on prepared powders. ∗ corresponds to diffraction peaks from the holder Be window. In situ data were originally collected at Co $K\alpha_1$ wavelength and recalculated at Cu $K\alpha_1$. Corresponding voltage−composition profile is given on the left.

taneously generated by the latter. This splitting is confirmed by the analysis of the in situ X-ray diffraction patterns series from 3.5 to the end of the discharge (4.75 lithium) depicted in Figure 3d. At this stage, Li_4ZnP_2, Zn, and $LiZn_4$ peaks rapidly disappear and only those characteristic of the final products, Li_3P[33] and LiZn, remain. LiZn diffraction peak positions, especially that of the (2, 2, 0) peak at 41.8° 2θ for $x = 3.75$, slightly differs from the 40.99° 2θ reported for pure LiZn and could be characteristic of a nonstoichiometric Zn-rich LiZn alloy. The progressive shift from 41.8° 2θ at $x = 3.75$ to 41.3° 2θ at $x = 4.75$ is associated with Li insertion into the LiZn matrix for a slight increase of the cell volume.

In situ XRD patterns and galvanostatic and potentiodynamic measurements demonstrate the multistep conversion mechanism of Zn_3P_2 to LiZn and Li_3P to be partially reversible. Moreover, in comparison to the discharge, the charge process appears rather simple (Figure 5). About half a lithium to one lithium are first extracted from LiZn by a solid solution process as demonstrated by the (2, 2, 0) peak shift from 41.3° 2θ for $x = 4.75$ to 41.82° 2θ for $x = 3.85$. On further Li extraction (starting from $x = 4.13$), LiZn is converted back into $LiZn_4$ following a simple two-phase process. At lithiation (or lithium extraction) stage corresponding to $x = 3.38$, Zn diffraction peaks quickly appear and then remain until the end of the charge. After extraction of about half lithium and the corresponding extraction of 0.25 Zn metal from $LiZn_4$, Zn peak intensities reach a

(33) JCPDS 74-1160.

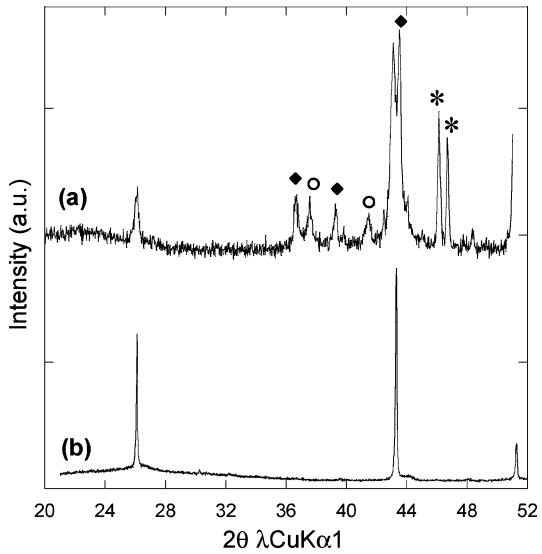

Figure 4. Comparison of X-ray diffraction patterns of Li_4ZnP_2 from in situ data (a) and as prepared by BMA (b). In (a), Zn and $LiZn_4$ diffraction peaks are marked with black diamonds and open circles, respectively. ∗ corresponds to diffraction peaks from the holder Be window.

maximum and LiZnP diffraction peaks progressively increase. Zn metal progressively extracted from $LiZn_4$ simultaneously reacts with Li_3P to form LiZnP. At the end of the charge the composite electrode content is limited to LiZnP and Zn metal, which are then used as starting materials for further cycling.

In situ X-ray diffraction patterns of Zn_3P_2 HT powder show the same features and changes upon lithiation as BMA powders. BM powder crystallinity is too poor and its corresponding X-ray diffraction pattern is too badly resolved to allow any reliable investigations. Anyway, on the basis of the similarities in galvanostatic curves (Figure 2), mechanisms are assumed to be the same for HT, BMA, and BM powders. The complete reaction mechanism of lithium toward Zn_3P_2 is detailed in Figure 6.

2.2. Crystal Structures of Li_4ZnP_2 and $LiZn_4$. Crystal and molecular structures of Li_4ZnP_2 and $LiZn_4$ were solved by Rietveld refinements of their X-ray diffraction data on powders. The diffraction pattern of Li_4ZnP_2 powder was indexed on the basis of the 11 observable lines by running the DICVOL program.[34] Figures of merit for a cubic solution were quite good: $M(11) = 83.5$,[35] $F(11) = 21.1(0.0118, 44)$.[36] A rough cubic cell was found with $a = 5.9026(3)$ Å. A complete analysis of the observed lines with DTETA program and selection of the extinction rules led to the identification of two suitable space groups: $Fm\bar{3}m$ (No. 225) and $F\bar{4}3m$ (No. 216).[37] Anyway, both groups present close symmetry properties especially for the more symmetrical sites. Differences lie then specifically in $Fm\bar{3}m$ 8c tetrahedral sites which are split in 4c and 4d in the $F\bar{4}3m$ space group because of the inversion center. Both groups were used for structure refinements and the best results were obtained with the $Fm\bar{3}m$ space group. Li_4ZnP_2 was found to be isostructural with Li_9MPn_4 phases (with M = Ti, V,... and Pn = As, P) we recently described but differences in both stoichiometries proscribed any trivial solutions.[5,6] To build a first structural model, atoms were however located in the same sites as those for Li_9MPn_4 phases respectively in (0, 0, 0) 4a site for P and in ($^1/_4$, $^1/_4$, $^1/_4$) 8c for Zn and Li. A total occupancy of 4a sites led to a total number of 4 phosphorus per unit cell for $Z = 2$. Since the Li_4ZnP_2 stoichiometry imposes Zn/P = 1/2, two Zn were placed in tetrahedral 8c sites for one-fourth of the total site occupancy. Six positions were then still available in 8c sites for Li. As for Li_xMPn_4 phases, the remaining 2 Li would lie in half the 4b octahedral sites. On the other hand, Zn−P (or Li−P) distances at 2.55 Å extracted from this model were found consistent with corresponding distances at 2.46 Å in Zn_3P_2 and at 2.89 Å in LiZnP.

For the $LiZn_4$ diffraction pattern, the indexation using the DICVOL program of the first 12 diffraction lines led to a monoclinic solution with good figures of merit: $M(12) = 60.8$, $F(12) = 16.9(0.0169, 42)$. However, parameters $a = 2.7829$ Å, $b = 4.3940$ Å, $c = 2.7737$ Å, and $\beta = 120.021°$, with such close values for a and c and a β angle at 120° strongly suggest a hexagonal solution. Noteworthy is the fact that Zn metal crystallizes in a $P6_3/mmc$ hexagonal space group, with $a = 2.6591$ Å and $b = 4.9353$ Å.[29] A closer comparison of its X-ray diffraction pattern with that of $LiZn_4$ shows similar series of diffraction lines of comparable intensities but large shifts in 2θ angle. As has often been observed for metal alloys, $LiZn_4$ and Zn are isostructural compounds, a partial substitution of Zn by Li in the same crystallographic site inducing changes as evidenced by X-ray diffraction. A structural model was built for $LiZn_4$ with both Zn and Li in the ($^1/_3$, $^2/_3$, $^1/_4$) 2c site with a Li/Zn ratio equal to 0.28 (experimental).

For both Li_4ZnP_2 and $LiZn_4$, the above-described models were used as starting points for Rietveld refinements using the Jana program.[38] Backgrounds were extracted by polynomial interpolations. Pseudo-Voigt functions were used for peak shape profiles, and asymmetries at low angles were corrected. Conditions and details for the refinements are summarized in Table 1. Plots of experimental and calculated X-ray diffraction patterns as well as their differences after final Rietveld refinements are shown in Figure 7 together with corresponding perspective views of the crystallographic arrangements. For both Li_4ZnP_2 and $LiZn_4$, final atomic positions and isotropic thermal parameters are given in Table 1.

2.3. Potentiodynamic Studies. Potentiodynamic curve (Figure 8) for Zn_3P_2 BMA powder reveals the complexity of the involved electrochemical mechanism. Comparison with curves from BM and HT powders however confirms it as unique (see Supporting Information). In the following paragraph, potentials are given in volts, V vs Li^+/Li. Potentiodynamic curve from BMA Zn_3P_2 powder shows six peaks in reduction at 0.75, 0.52, 0.45, 0.37, 0.21, and 0.15 V and six in oxidation at 0.26, 0.31, 0.51, 0.68, 1.18, and 1.71 V, respectively. The peak at 0.75 V labeled as A in Figure 8 vanished during the second discharge and was

(34) Louer, D.; Louer, M. *J. Appl. Crystallogr.* **1972**, *5*, 271.
(35) De Wolff, P. M. *J. Appl. Crystallogr.* **1968**, *5*, 108.
(36) Smith, G. S.; Snyder, R. L. *J. Appl. Crystallogr.* **1979**, *12*, 60.
(37) DTETA: Norbert, A. *Rev. Chim. Miner.* **1969**, *6*, 687.
(38) Petricek, V.; Dusek, M.; Palatinus, L. *Jana2000. The crystallographic computing system*; Institute of Physics: Praha, Czech Republic, 2000.

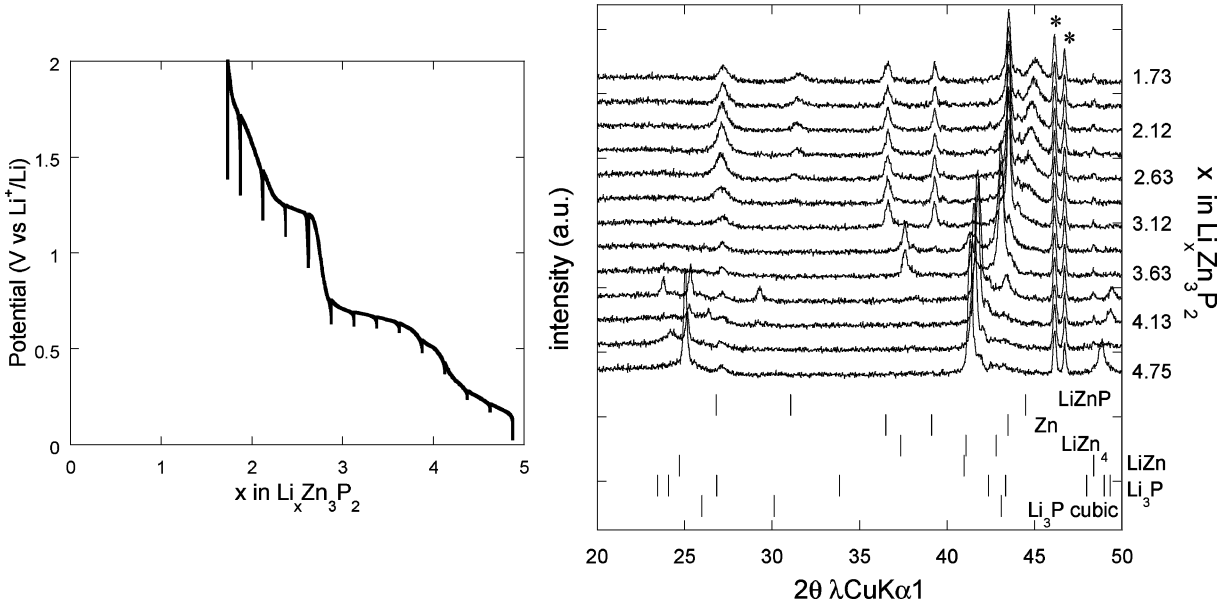

Figure 5. In situ X-ray diffraction patterns collected at various first charge states of lithiation for Zn_3P_2. Right axis gives corresponding Li composition. Bragg peak positions extracted from JCPDS database are given underneath experimental data for involved phases. For Li_4ZnP_2 and $LiZn_4$, Bragg peak positions were extracted from experimental X-ray diffraction data on prepared powders. ∗ corresponds to diffraction peaks from the holder Be window. In situ data were originally collected at Co $K\alpha_1$ wavelength and recalculated at Cu $K\alpha_1$. Central inset shows the corresponding voltage−composition profile.

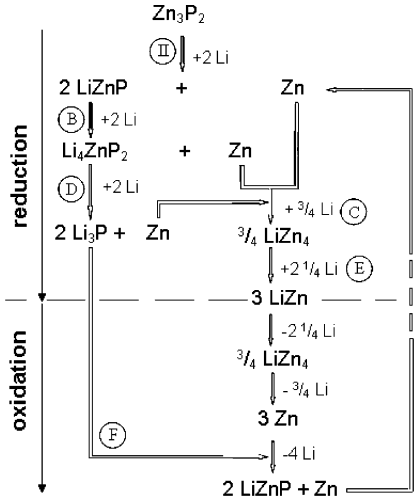

Figure 6. Schematic diagram of the overall electrochemical mechanism of Zn_3P_2 reaction with Li in discharge (up) and charge (down). Left part includes only phosphide phases while the right part corresponds to Zn−Li alloying and disalloying. Additional cycles do not involve Zn_3P_2 anymore. Potentiodynamic peak assignment is given as encircled letters (see Figure 3).

definitively associated with an irreversible phenomenon occurring only during the first discharge. As already observed, the peak definition of the curve improved from the first cycle to further cycles.[7] As a matter of fact, the B peak shoulder, labeled as II, was observed only during the first discharge while B peak intensity slightly decreased. Attempts for peak correspondences between reduction and oxidation have been extracted from potentiodynamic measurements done using various cutoff potentials. B and E peaks, strong and narrow in reduction, can be assigned to a biphasic phenomenon as demonstrated by the corresponding galvanostatic plateaus. The overall series of potential peaks observed in reduction remained however difficult to assign in oxidation. For a better assignment of the peaks, potentiodynamic measurements have also been done on pure Zn metal and prepared $LiZn_4$, LiZn, Li_4ZnP_2, and LiZnP (see Supporting Information).

A first cutoff potentiodynamic measurement performed with Zn_3P_2 BMA powder in the 2−0.7 V range showed a single peak (A) at 0.75 V in reduction with no correspondence in oxidation and characteristic of an irreversible process. Since A is observed only during the first sweep and disappears at further cycles, this peak was first associated with the irreversible conversion of Zn_3P_2 into LiZnP, which occurs only during the first discharge. A similar peak was however measured at the same potential values (≈0.75 V) in various Li−Zn−P prepared phases without any Zn_3P_2 content such as $LiZn_4$, Li_4ZnP_2, and LiZnP (see Supporting Information). Moreover, the Zn potentiodynamic curve shows a strong peak in reduction at this potential value and the A peak was definitively associated with the presence of Zn impurities in the prepared Zn_3P_2. For further lithiation, the B peak at 0.51 V was then assigned to the first electrochemical reaction of Li with Zn_3P_2, namely, the irreversible conversion of Zn_3P_2 into a mixture of LiZnP and extruded Zn metal. However, a cutoff experiment between 2 and 0.4 V confirmed the B peak remained present at 0.5 V for further cycles, inconsistent with an irreversible process as suggested by in situ data analysis. This peak at 0.5 V is actually obviously composite and the observed decrease of its measured width after a complete first cycle was first associated with the usually observed peak definition improvement in such potentiodynamic experiments. Moreover, a potentiodynamic experiment performed on BMA LiZnP powder showed an intense peak at 0.5 V in reduction with its correspondences in oxidation at 0.7 and 1.2 V (see Supporting Information). This latter point definitively assigns the B peak to both successive Zn_3P_2 to LiZnP and LiZnP to Li_4ZnP_2 conversions (plus Zn metal) occurring at the same potential. More precisely, the disappearance of the II-labeled shoulder and corresponding B peak narrowing during second

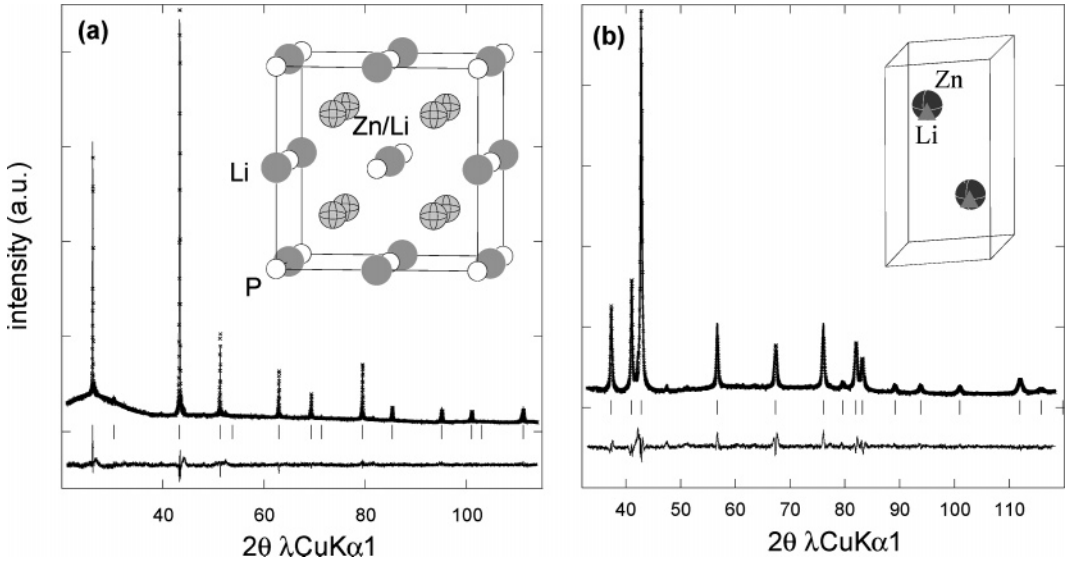

Figure 7. Observed (line), calculated (crosses), and difference plots and peak Bragg positions for Li_4ZnP_2 (a) and $LiZn_4$ (b) after the final refinements. Corresponding unit cells are included with phosphorus as the open circle, lithium as the light gray circle, and zinc and lithium sharing the same site as the decorated gray circle. $LiZn_4$ is depicted in an orthorhombic cell for sake of clarity (see Discussion section).

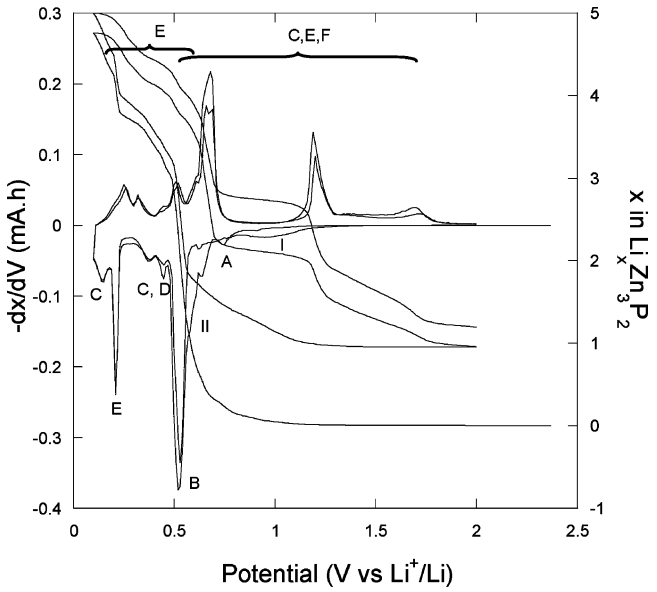

Figure 8. Potentiodynamic first two cycles together with corresponding galvanostatic curve at 10 mV/h and an equivalent of C/50 for Zn_3P_2(BMA)/Li in 2−0.1 V range.

and further cycles can be explained by the fact that since Zn_3P_2 is not recovered at the end of the cycle, B peak should then exclusively be assigned to the conversion of LiZnP into Li_4ZnP_2 for further cycles. To summarize, II corresponds to the irreversible conversion of Zn_3P_2 into LiZnP occurring only during the first sweep while B is assigned to LiZnP into Li_4ZnP_2 conversion under lithiation. Two small peaks, C and D, are more or less identified at low potential in the B peak base. Among the various involved species, only Zn and Li_4ZnP_2 have potentiodynamic incremental peaks in the 0.4−0.3 V range. Although they cannot be unambiguously assigned nor discriminated, C and D will be assigned respectively to Zn to $LiZn_4$ alloying and to the reduction of Li_4ZnP_2 into Li_3P. Zn alloying appears as a complex phenomenon and the low potential peak below 0.1 V observed in the potentiodynamic curve for Li reaction with Zn metal could correspond to a second contribution for C assigned in this low potential range. In oxidation, Zn disalloying shows a broad and undefined series of low-intensity potentiodynamic peaks in the 0.1−1 V range (see Supporting Information) and its contribution to Zn_3P_2 potentiodynamic measurement should be included in the curve background. The last reaction in reduction is the solid solution conversion of $LiZn_4$ in LiZn. The E potentiodynamic peak, sharp and intense, corresponds to this reaction. The potentiodynamic curve of pure $LiZn_4$ is rather simple with basically one single peak at 0.15 V in reduction. In contrast, oxidation appears as more complex with a broad and composite peak centered at 0.3 V and two peaks at 0.6 and 0.7 V (see Supplementary Information). However, this complex figure definitively allows the assignment of corresponding peaks of the Zn_3P_2 potentiodynamic curve.

We have not so far ascribed any obvious reversible reaction to potential peak #I but its progressive vanishing from BM to BMA and final disappearance from HT potentiodynamic curves suggest the associated reaction as strongly related to the powder morphology or crystallinity (see Supporting Information). Note that, as irreversible processes, corresponding reactions for A and D respectively the reaction of Li with Zn impurities and the reduction of Li_4ZnP_2 into Li_3P are obviously not observed in the oxidation part of the potentiodynamic curve. The various peak assignments and overall proposal pathway are schematically summarized in Figure 6 (encircled letters).

3. Discussion

The few examples of lithium reactions with binary transition metal phosphides available in the literature showed the insertion mechanism to mainly proceed by a progressive extraction of the metal, replaced within the phosphide matrix by Li^+ cations.[7,39,40] The discharge stops when no metal

(39) Alcantara, R.; Tirado, J. L.; Jumas, J. C.; Monconduit, L.; Fourcade, J. O. *J. Power Sources* **2002**, *109*, 308.
(40) Pralong, V.; Souza, D. C.; Leung, K. T.; Nazar, L. *Electrochem. Commun.* **2002**, *4*, 516.

cations are available for reduction and usually with the supposedly complete conversion of the initial phosphide into Li_3P. This was observed for CoP_3[39,40] and CuP_2,[41] for instance, for which Li_3P generation was accompanied by the reduction of metals as nanoparticles. For Cu_3P, the amorphous character of Li_3P formed at the end of the discharge did not allow any conclusive discrimination between Li_3P and a copper-poor lithium phosphide phase, i.e., $Li_{3-\epsilon}Cu_\epsilon P$.[7] In contrast, the charge usually proceeds by the reaction of Li_3P with generated metal particles to lead to defined ternary lithium-metal phosphide phases with low lithium content. However, low solid state reactivity of the metal and bond electronic characteristics within generated ternary phases explain the observed limitation in the reversibility of the overall oxidation process: initial binary phases are usually not recovered at the end of the charge. This partial reversibility accounts for the observed capacity loss from the first to the second sweep in such cells. Particle sintering and aggregation certainly also explain the observed performance fading upon cycling. Following this schema, since Li_3P (or related) is identified as the final product of the discharge, the phosphorus stoichiometry of the pristine binary compound leads the theoretical maximum number of "inserted" lithium to 3 times the initial phosphorus formulas content. Theoretical values are however to be evaluated with regard to experimental ones: 10 Li instead of 9 expected for CoP_3,[39] a bit less than 6 instead of 6 for CuP_2,[41] or 5 instead of 3 for Cu_3P, for instance.[7] Observed discrepancies could arise from various material limitations or specificities: less inserted lithium is associated with reactivity limitations while solid solution or solid electrolyte interphase (SEI) processes, for example, could originate for the reaction of more lithium than expected. The lithium insertion capabilities of the product(s) generated during the process can also advantageously impact electrode performances. As mentioned above, these intermediates are usually ternary lithium phosphide phases or extruded metals. Some of these ternary phases such as Li_xMP_4 (M = Ti, V, Mn...) can reversibly insert a large amount of lithium[5,6] but, except for MnP_4, none of such phases have so far been observed as intermediate in electrochemical processes for lithium insertion in binary metal phosphides.[42] Moreover, the conditions for MnP_4 recovery back at the end of the charge are still under discussion.[43] On the other hand, some transition metals are known to form lithium alloys. Zinc is one of these. Five different defined stoichiometries are referenced in the Li−Zn system: LiZn, $LiZn_2$, Li_2Zn_3, Li_2Zn_5, and $LiZn_4$.[11] With the description of the electrochemical mechanism of the reaction of Zn_3N_2 with lithium, Pereira et al. have demonstrated that each of these Li−Zn alloys can be involved in reversible lithiation processes.[17] Before this present work, LiZn was, in the series, the only one structurally described: it is a cubic $Fd\bar{3}m$ phase which is obtained by substitution of Zn by Li atoms in the $P6_3/mmc$ hexagonal matrix; this substitution induces the observed gain in the cell symmetry from hexagonal to cubic.[31] Our data have also confirmed $LiZn_4$, obtained by solid state reaction of Li with Zn nanoparticles, and LiZn both to greatly participate in the large specific capacity of Zn_3P_2 anodic material. On the basis of the described mechanism, the total capacity can be theoretically decomposed as the sum of two distinct contributions. After the reaction of about two Li with Zn_3P_2 to give a mixture of LiZnP and Zn metal, the lithiation proceeds on one side by the progressive replacement of Zn by Li in phosphide phases to give Li_4ZnP_2 and finally "Li_3P". The theoretical amount of lithium necessary to complete these reactions is equal to 4. On the other side, Zn metal, extruded at the various steps of the process, reacts with 3 Li to give 3 LiZn as a final product of the charge. This theoretical total of 9 "inserted" lithium cations should be compared to the 7 to 8 experimentally observed during the charge at C/13 and around 9 at C/190. On the other hand, the composition of the composite electrode after a complete cycle is a mixture of LiZnP and Zn in a 2/1 molar ratio. The irreversible capacity loss at the end of the first cycle should theoretically correspond to this unreacted Zn. In the whole series of prepared Zn_3P_2, galvanostatic curves in Figure 2 show the second sweep to roughly end at $x = 2$, confirming the good reversibility of other involved processes but the conversion of LiZnP back to Zn_3P_2. These roughly two lithium "lost" in the charge process correspond to a capacity loss of about 20−30% of the initial capacity at first sweep at C/13 and 30−40% at C/190 scan rate (Table 2). For further cycles, capacity fading is low, especially for the most crystallized BMA and HT powders: after 10 cycles the capacity is 88% of those at the first cycle for HT and 89% for BMA Zn_3P_2 powders. With BM Zn_3P_2 powder only 18% of the capacity at the first cycle is retained at the 10th cycle. Noteworthy is the fact that, quite unusually, capacity retention is worse at the C/190 low scan rate than that at C/13. Anyway, in such electrochemical mechanism processing during the charge by solid state reaction of metal particles generated during the discharge, particle sintering and aggregation upon cycling usually account for observed capacity fading: the bigger the metal particles, the lower their corresponding reactivity. For BMA and HT Zn_3P_2 powders, Zn is generated by reduction as nanocrystalline inclusions in a "crystallized" phosphide matrix limiting the particle aggregation before metal Li-alloying. In contrast, generated Zn particles are more easily extruded from Zn_3P_2 BM micronic particles during the discharge, allowing unfavorable sintering and inducing a faster capacity fading.

In situ X-ray diffraction data give a rather clear image of the complex electrochemical process of the reversible reaction of lithium with Zn_3P_2. In contrast potentiodynamic peaks are not easily assigned and X-ray diffraction data and electrochemical measurements remain difficult to correlate. Despite the complexity of the electrochemical reaction of Li with Zn_3P_2, as described to proceed by two distinct and parallel pathways, the electrochemical mechanism appears as highly reversible. This reversibility arises thanks to the strong structural relationship between the various involved phases. Figure 9 depicts the crystallographic relations starting

(41) Wang, K.; Yang, J.; Xie, J.; Wang, B.; Wen, Z. *Electrochem. Commun.* **2003**, *5*, 480.
(42) Souza, D. C.; Pralong, V.; Jacobson, A. J.; Nazar, L. F. *Science* **2002**, *296*, 5575.
(43) Gillot, F.; Monconduit, L.; Doublet, M. L. *Chem. Mater.* **2005**, *17*, 5817.

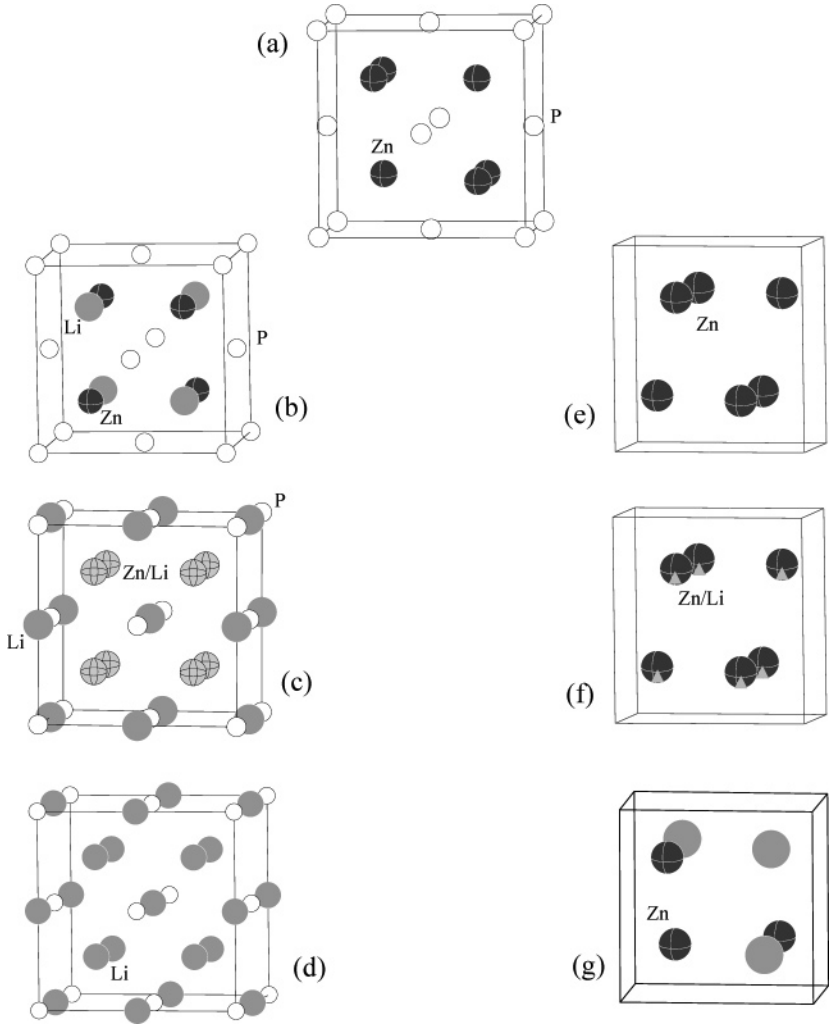

Figure 9. Perspective views of various phases involved in the electrochemical process of lithium reaction with Zn_3P_2: (a) Zn_3P_2, (b) LiZnP, (c) Li_4ZnP_2, (d) cubic Li_3P (or $Li_{3-2\epsilon}Zn_\epsilon P$), (e) Zn, (f) $LiZn_4$, and (g) LiZn. Phosphorus as the open circle, lithium as the light gray circle, zinc as the gray circle, and zinc and lithium sharing the same site as the decorated gray circle. $LiZn_4$ is depicted in an orthorhombic cell for sake of clarity (see Discussion section).

from Zn_3P_2 and then between phosphides, LiZnP, Li_4ZnP_2, and Li_3P on one side and Zn, $LiZn_4$, and LiZn on the other. Zn_3P_2 was first described as cubic[24] but our prepared form is a tetragonal $P4_2/nmc$ (No. 137) cell ($a = 8.0889$ Å, $c = 11.4069$ Å).[22,23] It can also be described in a smaller and quasi-cubic $P4_2/n$ cell ($a = 5.72$ Å, $c = 5.70$ Å) with phosphorus atoms at the corner and center of the faces (quasi fcc) while Zn occupy three-fourths of the tetrahedral sites.[25] Note that, without any consideration for octahedral sites, two tetrahedral sites per cell remain available for Li insertion in this open framework through a solid solution process. From Zn_3P_2 (or slightly Li-inserted Zn_3P_2) to LiZnP as the first phosphide phase formed upon discharge, the cell slightly increases its volume and gains symmetry by becoming an $F\bar{4}3m$ cubic cell ($a = 5.7790$ Å).[44,45] From Zn_3P_2 arrangement, the phosphorus fcc network remains but two zinc other six are excluded from the tetrahedral sites. Four Li/cell are inserted in available tetrahedral sites for a 1/1 Li/Zn ratio. Upon further lithiation, Zn cations keep on being extracted from the cubic cell and are replaced by Li^+ in the tetrahedral sites. When no room is available in the tetrahedral sites, as is the case for Li_4ZnP_2 (or $Li_8Zn_2P_4$ since $Z = 2$) with 6 Li and 2 Zn for a total occupancy of tetrahedral sites, additional Li (2) are inserted for a partial occupancy of the octahedral sites. Li_4ZnP_2 can then be rewritten as $Li^{Oh}Li_3^{Td}ZnP_2$. Note that the statistical disorder in tetrahedral site occupancies undergoing the LiZnP into Li_4ZnP_2 conversion induces a gain in the cubic cell symmetry from $F\bar{4}3m$ to $Fm\bar{3}m$. Additional Li to replace Zn in tetrahedral sites and to occupy octahedral sites could lead to an $Fm\bar{3}m$ cubic Li_3P cell while Li_3P is actually known to crystallize in a hexagonal cell. The last lithiation step in metal pnictide binary phases has often been described as complicated. For example, the discharge mechanism of the Li reaction with Zn_3N_2 has been shown to end with the formation of high-pressure Li_3N β form instead of the usually observed low-temperature−low-pressure α form.[17] Both Li_3N structures are hexagonal but, in contrast, while the low-temperature−low-pressure Li_3P form is hexagonal, a cubic Li_3P form is obtained under pressure.[46] On the other hand, starting from Cu_3P, any hexagonal Li_3P could not be evidenced using in situ X-ray diffraction and an amorphous $Li_{3-\epsilon}Cu_\epsilon P$ was suggested as the final product of the discharge.[7] A similar suggestion can be made in the present

(44) El Maslout, A.; Motte, J. P.; Gleitzer, C.; Aubry, J. *J. Solid State Chem.* **1973**, *7*, 250.
(45) Nowotny, H.; Bachmayer, K. *Monatsh. Chem.* **1950**, *81*, 488.
(46) Leonova, M. E.; Bdikin, I. K.; Burdina, S. A. *Inorg. Mater.* **2003**, *39*, 266.

case since the complexity of in situ X-ray diffraction data at the end of the discharge do not allow any discrimination to be reached between hexagonal Li_3P or cubic Li_3P or $Li_{3-2\epsilon}Zn_\epsilon P$. The last two cubic structures are however considered as more consistent with the described mechanism.

The conversion of Zn_3P_2 in LiZnP also proceeds by Zn extraction. Zn crystallizes in a hexagonal cell but can also be depicted in a *Cmcm* orthorhombic cell for a better understanding of the structural transformation: The Zn cell can then be described as a P-naked Zn_3P_2 cell with Zn remaining in originally tetrahedral sites. This conversion induces a shift of Zn planes in the [1 0 0] direction as exhibited by the Zn_3P_2 cubic to Zn hexagonal (orthorhombic) cell conversion. Zn−Zn distances, originally at about 2.85 Å in the pristine quasi-cubic cell, are then obviously not equivalent anymore with a split at 2.665 Å in the (0 0 1) plane while dZn−Zn = 2.913 Å in the (0 −3 1) plane. Meanwhile, the Zn−Zn−Zn angle goes from 90° to 117.2° close to a 120° hexagonal angle. $LiZn_4$ is obtained by replacing one-fifth of the Zn atoms in the original Zn metal hexagonal cell. A slight volume change from 30.43 $Å^3$ for the Zn cell to 29.35 $Å^3$ for $LiZn_4$ takes place in this substitution. Further lithiation of $LiZn_4$ induces a drastic cell symmetry change as a cubic cell is recovered at this step. This conversion is obtained by a shift of the (Li,Zn) planes in the [1 0 0] direction back to the cubic arrangement. At this stage, lithiation proceeds by the progressive replacement of Zn by Li in tetrahedral sites in an $Fd\bar{3}m$ cubic structure closely related to that of LiZn.[31] This solid solution process from $Li_{1+2\alpha}Zn_{4-\alpha}$ (with $0 < \alpha \leq 1$) to LiZn is exhibited by the peak shift observed in corresponding in situ X-ray diffraction patterns (Figure 3d). For sake of clarity, the cubic LiZn is depicted in Figure 9g on the basis of a repetitive unit built from 3 Zn and 3 Li atoms lying in pseudo-tetrahedral sites.

At the beginning of the charge, reverse reactions occur and oxidation proceeds by lithium extraction from LiZn to give Zn metal through the intermediate formation of $LiZn_4$. The last oxidation step corresponds to the solid-state reaction of Zn metal with Li_3P. Resulting LiZnP can easily be described as cubic Li_3P in which half the tetrahedral lithiums are replaced by zinc cations or vice versa, as the orthorhombic Zn cell decorated with phosphorus at the corner, center of the faces, and center of the cell and in which Zn's are partially replaced by Li in a 1/1 Li/Zn ratio. Finally, only the structural resemblances among all the various phases involved in the electrochemical process, independently from the pathway they belong to, account for the high reversibility of the overall electrochemical mechanism.

Concluding Remarks

The electrochemical mechanism of Zn_3P_2 reaction toward lithium leads to high first capacity values up to 995 (mA h)/g or 4519 (mA h)/cm^3. Although capacity at the following discharge decreases down to 666 (mA h)/g (3025 (mA h)/cm^3), these values have to be compared to graphite capacities respectively at 372 (mA h)/g and 830 (mA h)/cm^3.[47,48] Excluding Zn and Li−Zn alloys contribution to the electrochemical process, and considering only phosphide phases for a progressive conversion by Zn extraction of Zn_3P_2 into Li_3P, the corresponding theoretical capacity values are limited to 536 (mA h)/g and 2435 (mA h)/cm^3. This points out the interest of lithium ion electrode materials based on binary phosphide phases including transition metal which can reversibly form Li-metal alloys.

The various phases involved in the overall reaction are structurally close, allowing a high reversibility of the process, and despite the complexity of the electrochemical mechanism, the potential range from 1.25 to 0.1 V is suitable for the use of Zn_3P_2 as a negative electrode. Some of the observed transitions certainly disfavor the electrochemical performances of these materials, especially on capacity retention. A better control of the powder morphology and sampling, and of the electrochemical parameters, such as scan rate and potential window, will certainly help to improve these performances.

Acknowledgment. CNRS is gratefully acknowledged for funding. M.P.B. thanks the staff from "Unité de Prototypage" for its kind help during her stay in Amiens (France). Authors thank M. L. Doublet and L. Monconduit for helpful discussions.

Supporting Information Available: Figures showing potentiodynamic first cycles and CIF files for Li_4ZnP_2 and $LiZn_4$ zinc phosphides. This material is available free of charge via the Internet at http://pubs.acs.org.

CM0513379

(47) Flandrois, S.; Simon, B. *Carbon* **1999**, *37*, 165.
(48) Yazami, R. *Electrochim. Acta* **1999**, *45*, 87.